Materials Advances

ROYAL SOCIETY OF CHEMISTRY

PAPER

View Article Online
View Journal | View Issue



Cite this: *Mater. Adv.*, 2022, 3, 4699

# Photocatalytic conversion of arylboronic acids to phenols by a new 2D donor–acceptor covalent organic framework†

Bingcai Luo,‡ Yubao Zhang,‡ Ying Chen and Jianqiang Huo *

Covalent organic frameworks (COFs) are a kind of promising crystalline material for photocatalytic organic conversion. The introduction of electron donor–acceptor (D–A) units into its structure can reasonably adjust the photoelectric properties and energy bandwidth of COFs. In this research, we designed and synthesized a two-dimensional (2D) D–A type COF (**BTT-BTDDA-COF**) based on alternating connections of benzotrithiophene (BTT) and 4,4′-(2,1,3-benzothiadiazole-4,7-diyl)dianiline (BTDDA) units, with a wide visible light absorption range and good photoelectric response characteristics. In the photocatalytic conversion of arylboronic acid to phenol, **BTT-BTDDA-COF** exhibits high catalytic activity, wide substrate applicability and good recoverability. The high-efficiency photocatalytic activity of **BTT-BTDDA-COF** is reasonably attributed to the electron push–pull effect between the donor and acceptor units, which significantly improves the transfer and separation of carriers, which leads to the expansion of the visible light absorption range. The above results show the practicability of COFs material design and provide a new idea for the application of the new D–A COF catalyst in photocatalytic organic conversion.

Received 1st March 2022,
Accepted 9th April 2022

DOI: 10.1039/d2ma00237j

rsc.li/materials-advances



## 1. Introduction

The increasingly serious global energy crisis and ecological environmental pollution have become the greatest threat to human society today.[1] Solar energy as one of the most abundant renewable energies provides a new way to solve these problems.[2] The development of photocatalytic materials with the advantages of low energy consumption and being pollution-free is the most critical key factor.[3] Researchers have conducted many explorations on inorganic semiconductor materials with clear energy band structures such as $TiO_2$,[4] ZnO,[5] and $MoS_2$,[6] and found that they have good absorption of light in the ultraviolet region. At the same time, in order to improve the photocatalytic performance and expand the absorption range of visible light, the research of organic photocatalysts such as organic dyes,[7] *g*-$C_3N_4$,[8] MOFs[9] and COFs[10–16] has gradually attracted people's attention. In contrast, COFs are often used as a photocatalytic material because of their good chemical stability and adjustable chemical structure.[17–24]

With extended π-conjugated frameworks, excellent stability and adjustable chemical structures, COFs have shown great potential for broad applications in many prospects, such as phototransistors, optoelectronic devices and photocatalytic reactions.[25–32] Recently, reactions like redox, CH functionalization and E/Z isomerization have proved that covalent organic frameworks have great appeal in visible light-driven organic transformations.[33–37] They provide a simple and environmentally friendly method for the synthesis of important chemicals. At present, a variety of COFs catalysts have been developed by researchers and are still being explored. Consequently, it is necessary to design and synthesize COFs catalysts with high photocatalytic activity. Generally, a high-efficiency photocatalyst should have a wide light absorption range, an appropriate band gap, and effective charge transport capabilities. A feasible method is to design a COF with alternately connected electron donor–acceptor units in the framework through a reasonable molecular design strategy.

The design and construction of a COF with a donor–acceptor (D–A) structure has been proved to be an effective method to reduce the band gap and accelerate the intramolecular charge transfer.[38–42] However, the current research on COFs reports low catalytic efficiency and limited selection.[43–48] Through a literature review, we found that the bottom-up design method provides great possibilities for the synthesis of new high-performance COF catalysts.[23,49–58] As is well known, the

*College of Chemistry and Chemical Engineering, Key Laboratory of Eco-functional Polymer Materials of the Ministry of Education, Key Laboratory of Eco-environmental Polymer Materials of Gansu Province, Northwest Normal University, Lanzhou 730070, P. R. China. E-mail: huojianqiang@hotmail.com*

† Electronic supplementary information (ESI) available. See DOI: https://doi.org/10.1039/d2ma00237j

‡ These authors contributed equally to this work.

4,4′-(2,1,3-benzothiadiazole-4,7-diyl)dianiline (BTDDA) unit is currently one of the most effective electron acceptors. It can adjust the band gap and improve the charge separation and transfer properties of polymers. In addition, the pairing of BTDDA and electron-rich units can lead to significant delocalization of charges within the conjugated framework molecule, and the resulting polymer exhibits a narrower band gap and enhanced light absorption in the near-infrared region. Our previous study[59] has shown that the benzotrithiophene (BTT) unit can be designed as an efficient COF photocatalyst and has good photosensitivity.

As a proof of inspiration, a new COF (**BTT-BTDDA-COF**) was successfully synthesized from electron donor unit benzotrithiophene (BTT) and electron acceptor unit 4,4′-(2,1,3-benzothiadiazole-4,7-diyl)dianiline (BTDDA) through the bottom-up Schiff base reaction. The new COF constitutes a D–A type structure. Meanwhile, the structural composition and photocatalytic organic conversion performance have been studied. As expected, **BTT-BTDDA-COF** provides a suitable energy band structure, strong visible light absorption capacity and fast electron migration rate, making it a highly active photocatalyst. As a matter of course it is applied in the photocatalytic conversion of aryl phenyl boronic acid to phenol.[10,58,60–66] It exhibits high-efficiency catalytic performance and good recyclability. This work emphasizes the importance of constructing a well-defined D–A structure for the effective design of COF photocatalysts, and provides an effective strategy for the further design and synthesis of more efficient COF photocatalysts.

## 2. Experimental section

### 2.1 Materials and methods

All other reagents and solvents are analytically pure and can be used directly without further purification. X-ray photoelectron spectroscopy measurement was performed using an instrument (ThermoFisher Scientific, ESCALAB250Xi, USA). A CH Instruments 660E electrochemical workstation was used to test the photoelectric performance of the samples. $^{1}$H NMR and $^{13}$C NMR spectra were recorded with an Agilent 600 MHz spectrometer. FT-IR spectra were recorded from 400 to 4000 cm$^{-1}$ by using KBr pellets on a DIGILAB FTS-3000 spectrometer. Powder X-ray diffraction (PXRD) patterns were taken on a D/max 2200PC diffractometer at room temperature. Morphology analysis was performed using an ULTRA Plus scanning electron microscope (SEM). Thermogravimetric analysis (TGA) was performed on a NETZSCH Instruments thermal analyzer (STA449C) from 25 to 800 °C at a heating rate of 10 °C min$^{-1}$ under an $N_2$ atmosphere. $N_2$ adsorption–desorption isotherms were measured on an Autosorb iQ Station (QuantaChrome Instruments V 5.0) at 77 K, and the Brunauer–Emmett–Teller (BET) method was utilized to calculate the specific surface areas and pore volume. The UV-vis absorption spectra were recorded on an Agilent 8453 UV-vis spectrophotometer.

### 2.2 Synthesis of BTT-BTDDA-COF

The synthesis method of **BTT-BTDDA-COF** is shown in Scheme 1. BTT (66.1 mg, 0.2 mmol) and BTDDA (95.5 mg, 0.3 mmol) were placed in a heat-resistant glass bottle with 1,4-dioxane (3 mL), methylene (3 mL) and 6 M AcOH (0.3 mL), respectively. After ultrasonic dispersion for 5 min, the mixture was sealed in an $N_2$ atmosphere and heated at 120 °C for 3 days. After cooling to room temperature, the products were separated by centrifugation, washed with DMF, methanol and ethanol several times successively, and then Soxhlet extracted with THF for 24 h. Finally, the solid obtained was dried at 100 °C under vacuum for 12 h to obtain the red **BTT-BTDDA-COF**.

## 3. Results and discussion

### 3.1 Fourier transform infrared spectroscopy characterization

Through the FT-IR spectrum (Fig. 1(a)), we can find that a new imine bond (–C═N–) stretching vibration peak appears at 1608 cm$^{-1}$, The amino group (–$NH_2$) at 3364 cm$^{-1}$ and the stretching vibration peak of the aldehyde group (–CHO) of

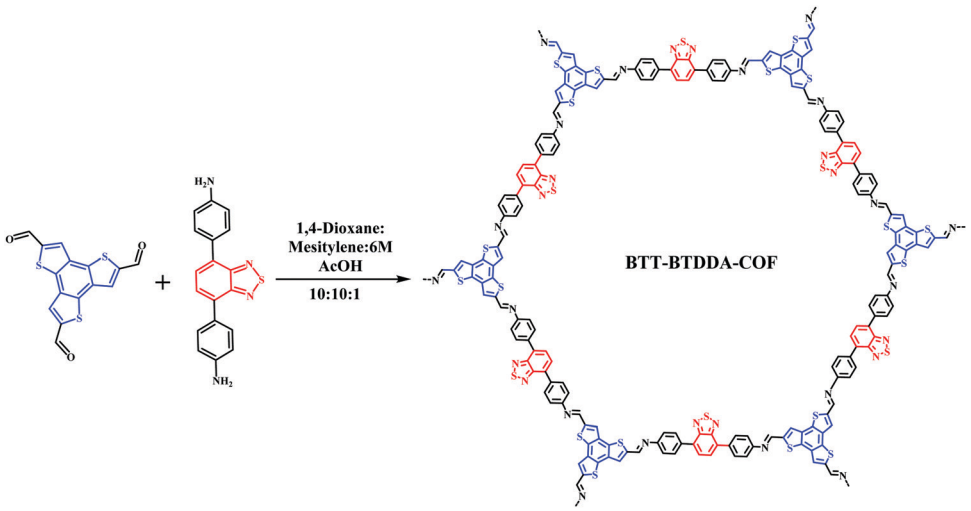


Scheme 1 The synthetic route of **BTT-BTDDA-COF**.

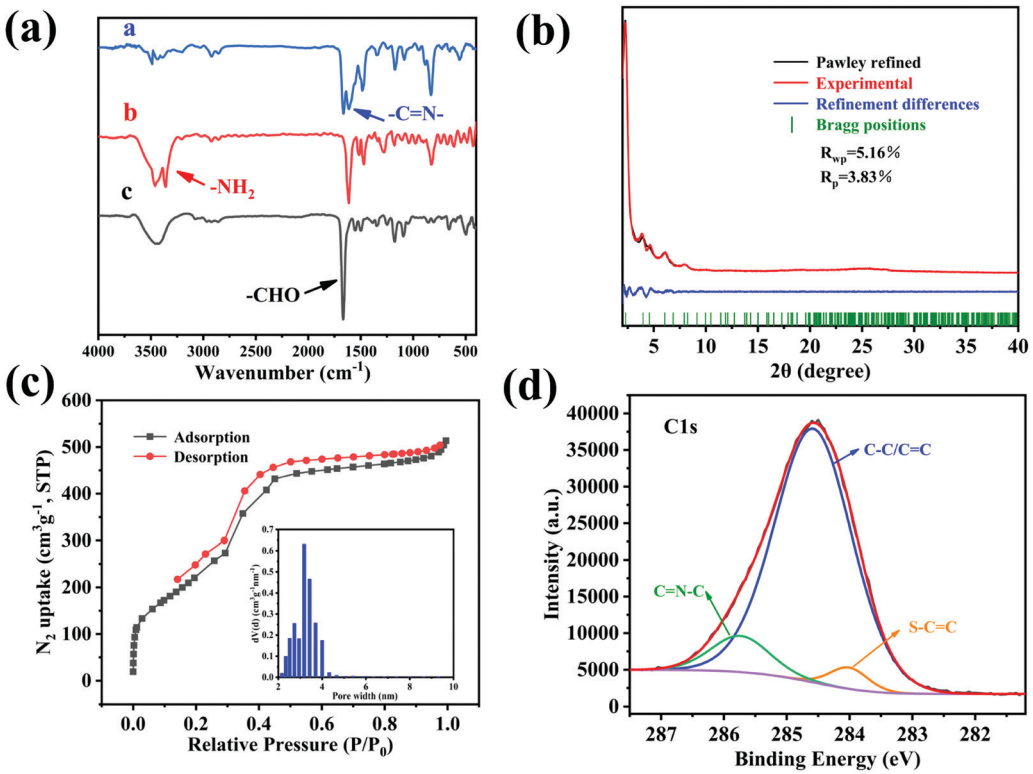


Fig. 1 (a) FT-IR spectra of **BTT-BTDDA-COF** (a), BTDDA (b), and BTT (c); (b) PXRD patterns of **BTT-BTDDA-COF** (red) with the corresponding Pawley refinement (black) indicating negligible differences (blue) to the experimental data [$R_{wp}$ = 5.16% and $R_p$ = 3.83%]; (c) $N_2$ absorption–desorption isotherms of **BTT-BTDDA-COF** and pore size distribution plot (inset); (d) high-resolution XPS C 1s spectra of **BTT-BTDDA-COF**.

1665 $cm^{-1}$ have basically disappeared, indicating that the two monomers have formed **BTT-BTDDA-COF** through the condensation reaction of the aldehyde and amine.

### 3.2 Powder X-ray diffraction (PXRD) analysis

The structure of **BTT-BTDDA-COF** is simulated by Materials Studio software (Fig. 2) and Pawley refinement of PXRD (Fig. 1(b)). As shown in Fig. S2 (ESI†), **BTT-BTDDA-COF** has a strong diffraction peak at 2.32°, and four different diffraction peaks at 4.02°, 4.64°, 6.12° and 8.02°, which correspond to 100, 110, 200, 120 and 220 crystals, respectively. In addition, through Pawley refinement, a unit cell with space group *P*6 is obtained, the parameters are $a$ = 44.277 Å, $b$ = 44.277 Å, $c$ = 4.3087 Å and $\alpha$ = 90°, $\beta$ = 90°, $\gamma$ = 120° (Table S1, ESI†),

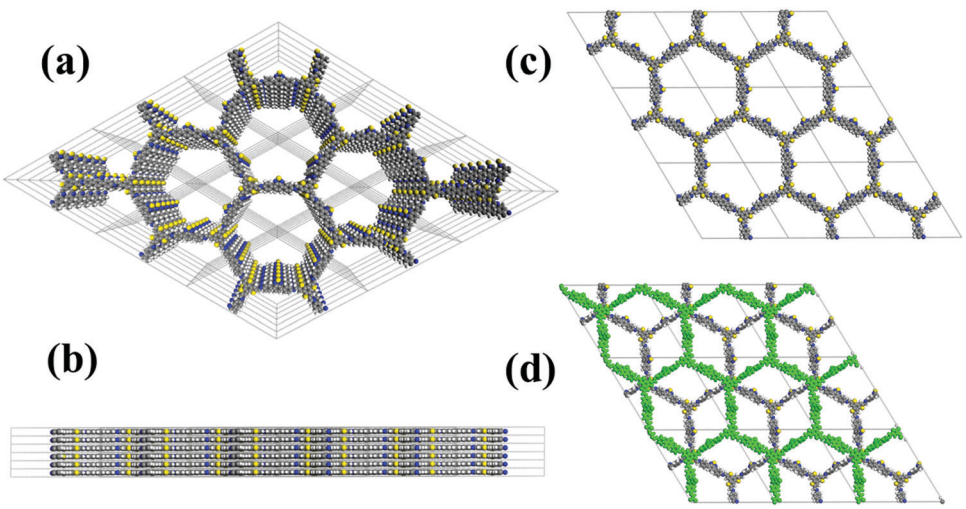


Fig. 2 (a) Top and (b) side views of **BTT-BTDDA-COF** in the simulated AA eclipsed stacking model. (c) AA eclipsed stacking model for **BTT-BTDDA-COF**. (d) AB staggered stacking model for **BTT-BTDDA-COF**.

where $R_{wp}$ = 5.16% and $R_p$ = 3.83%. Compared with staggered AB stacking, the simulated PXRD pattern of overlapping AA stacking (Fig. S2, ESI†) is more consistent with the experimental data.

### 3.3 Surface area measurement

The porosity and surface area of **BTT-BTDDA-COF** were measured by nitrogen adsorption–desorption experiments at 77 K. As shown in Fig. 1(c), the specific surface area of **BTT-BTDDA-COF** is 908.9257 $m^2\ g^{-1}$. The pore size calculated by non-local density functional theory (NLDFT) is mainly distributed at 3.83 nm (Fig. 1(c)), which is basically consistent with the theoretical data (3.96 nm) obtained by the AA stacking model, which further shows that the **BTT-BTDDA-COF** with an excellent network structure was successfully synthesized.

### 3.4 Surface morphology analysis

The surface morphology of **BTT-BTDDA-COF** was analyzed by SEM and TEM. Fig. S1(d–f, ESI†) is SEM images of **BTT-BTDDA-COF** at different magnifications. The SEM images show that **BTT-BTDDA-COF** has an irregular rod shape. EDS analysis (Fig. S1(g–k), ESI†) proves that C, N, and S elements are evenly distributed in the COF material, which is basically consistent with the results of XPS analysis. It can be seen from TEM (Fig. S1(a–c), ESI†) that **BTT-BTDDA-COF** has clear lattice fringes, which further confirms the high crystallinity of **BTT-BTDDA-COF**.

### 3.5 X-Ray photoelectron spectroscopy (XPS) characterization

In order to prove the element types and valence states on the surface of **BTT-BTDDA-COF** we carried out XPS tests. As shown in Fig. S3 (ESI†), the main constituent elements of **BTT-BTDDA-COF** are C, N, and S.[24,67–69] The C 1s peak at 284.58 eV is a carbon atom in the benzene ring, while the two C 1s peaks at 284.01 and 285.74 eV are derived from thiophene units and imine bonds, respectively (Fig. 1(d)). The XPS and FTIR results provide enough information about the structure of **BTT-BTDDA-COF** and prove that **BTT-BTDDA-COF** has been successfully synthesized.

### 3.6 Stability analysis

Considering the application range of the material, we explored the solvent stability and thermal stability of **BTT-BTDDA-COF**. Thermogravimetric analysis (Fig. 3(a)) shows that under a nitrogen atmosphere, **BTT-BTDDA-COF** can maintain a stable structure at a high temperature of 304.3 °C. In addition, the stability of the photocatalyst is also reflected in the material's good tolerance to solvents. Subsequently, at 25 °C, **BTT-BTDDA-COF** was soaked in different solutions for 3 days including *N*,*N*-dimethylformamide (DMF), ethanol, HCl (pH = 1) aqueous solution and NaOH aqueous solution (pH = 13). The solvent stability of **BTT-BTDDA-COF** was characterized by PXRD. It can be seen from the comparison of Fig. 3(b), that the position and intensity of each diffraction peak of **BTT-BTDDA-COF** before and after immersion in different solvents remain basically unchanged, which proves that it is stable in various solutions. Therefore, **BTT-BTDDA-COF** exhibits excellent thermal and chemical stability, which expands its application range in the field of photocatalysis.

### 3.7 Photoelectric performance analysis

In order to study the optical properties of the material, the obtained **BTT-BTDDA-COF** was firstly analyzed by solid UV-vis diffuse reflectance spectroscopy (DRS). As shown in Fig. 4(a), **BTT-BTDDA-COF** shows a wide absorption peak of visible light, with the edge of the absorption band extending into the near infrared region. The wide absorption and narrow energy gap may be attributed to efficient intramolecular charge transfer from donor to recipient. In addition, BTT and BTDDA units also improve the conjugation degree in the system at the molecular level, which further promotes the carrier flow and reduces the band gap. The optical band gap was calculated as 1.99 eV by Tauc diagram. In order to further study the relative position of the valence band (VB) and conduction band (CB), XPS-VB analysis was carried out and the valence band value was 1.02 eV (Fig. S4(a), ESI†), and CB was calculated as −0.97 eV. It can be found by comparison (Fig. S4(b), ESI†) that **BTT-BTDDA-COF** is sufficient to reduce $O_2$ to $O_2^{\bullet-}$ (−0.33V *vs.* NHE). Obviously, THE $E_{VB}$ of **BTT-BTDDA-COF** fully meets the above criteria. In addition, the PL strength of **BTT-BTDDA-COF** is much weaker

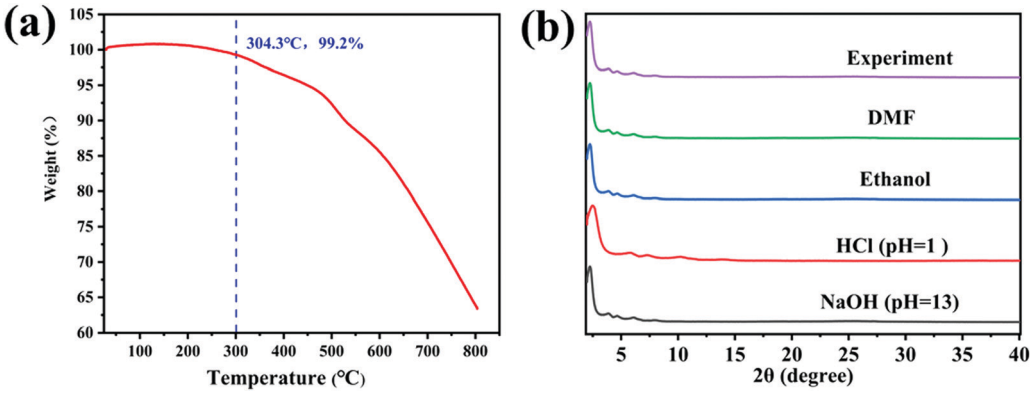


Fig. 3 (a) TGA diagram; (b) PXRD diagram (solvent stability).

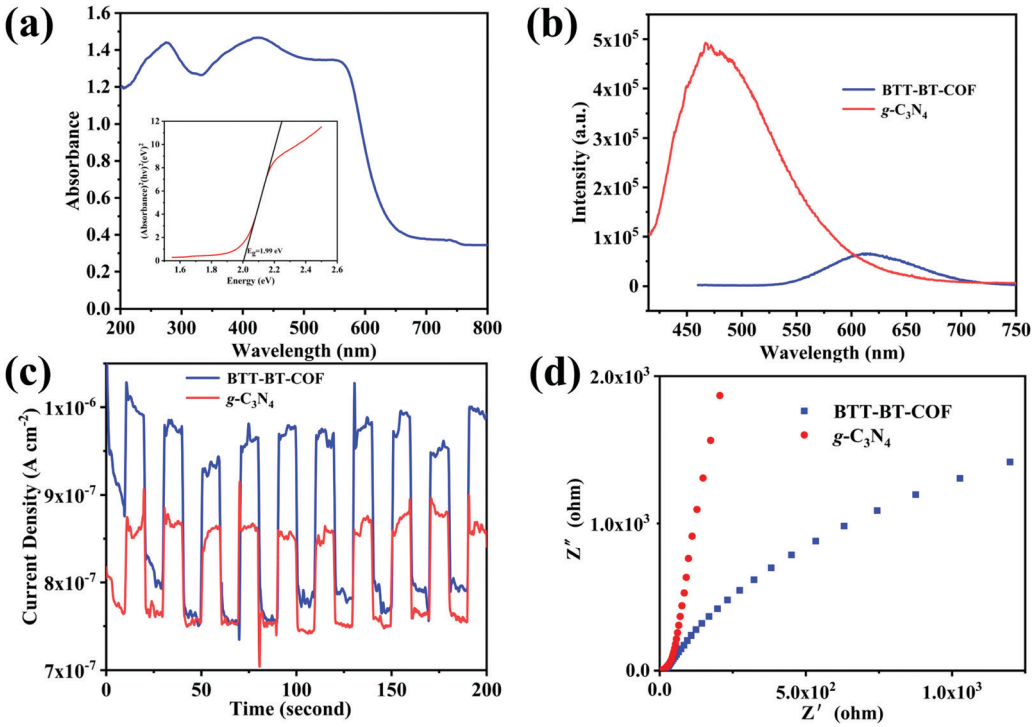


Fig. 4 (a) Solid-state UV-Vis spectra of **BTT-BTDDA-COF**; (b) photoluminescence spectra of $g$-$C_3N_4$ and **BTT-BTDDA-COF**; (c) transient photocurrent response diagrams of **BTT-BTDDA-COF** and $g$-$C_3N_4$ under light irradiation; (d) impedance diagrams of **BTT-BTDDA-COF** and $g$-$C_3N_4$.

than that of $g$-$C_3N_4$ (Fig. 4(b)), which indicates that the recombination of **BTT-BTDDA-COF** photogenerated carriers is inhibited and has a high photoinduced electron hole pair separation efficiency.

**BTT-BTDDA-COF** shows a fast photocurrent response under repeated cycles of visible illumination and multiple intermittent switching illuminations (Fig. 4(c)). Compared with $g$-$C_3N_4$, the **BTT-BTDDA-COF** photocurrent response is significantly enhanced, indicating that **BTT-BTDDA-COF** photogenerated charge can be separated more effectively. In addition, we also found that the photocurrent density of **BTT-BTDDA-COF** does not decay with the increase of the illumination time, which means that **BTT-BTDDA-COF** can provide a stable number of photogenerated electrons and holes during the illumination process. As can be seen from the EIS Nyquist diagram (Fig. 4(d)), compared with $g$-$C_3N_4$, **BTT-BTDDA-COF** has a smaller arc radius, indicating that it has a higher conductivity, thus enhancing the ability of electron transfer in the photocatalyst.

### 3.8 Study on the photocatalytic performance of BTT-BTDDA-COF

Triethylamine (as sacrifice electron donor) (0.3 mmol), catalyst **BTT-BTDDA-COF** (2 mg) and substrate benzenboric acid (0.1 mmol) were added into a transparent glass bottle filled with 3 mL acetonitrile. Under the irradiation of a 36 W blue LED lamp, phenol was separated and obtained after 26 h of reaction in an air atmosphere, with a yield of 93% (Table 1 entry 1). By comparison, we found that the reaction did not occur

Table 1 Optimization of the reaction conditions

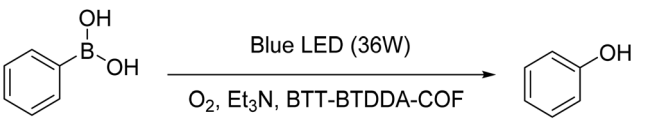


| Entry[a] | Catalyst | Reaction condition variations | Yield[b] (%) |
|---|---|---|---|
| 1 | **BTT-BTDDA-COF** | No change | 93 |
| 2 | **BTT-BTDDA-COF** | No light | $<5$ |
| 3 | **BTT-BTDDA-COF** | No $O_2$ ($N_2$) | Trace |
| 4 | **BTT-BTDDA-COF** | No $Et_3N$ | Trace |
| 5 | **BTT-BTDDA-COF** | benzoquinone | 20 |
| 6 | — | No change | Trace |
| 7 | BTT | No change | 30 |
| 8 | BTDDA | No change | 10 |

[a] Reaction conditions: phenylboronic acid (0.1 mmol), photocatalyst (2 mg), $Et_3N$ (0.3 mmol), 3 mL $CH_3CN$, air, 26 h, Blue LED (36 W). [b] Isolated yield.

without the addition of photocatalyst (Table 1, entry 6), indicating that **BTT-BTDDA-COF** plays a decisive role in the catalytic reaction. We also tested the catalytic effect of BTT and BTDDA units on arylboronic acid. It can be seen from Table 1 entries 7 and 8 that BTT shows a low conversion rate (30%), while the BTDDA unit only has a 10% conversion rate, indicating that the structure of the D–A Type COF plays a key role in the catalytic reaction. A series of subsequent controlled experiments showed that the reaction was difficult to occur in the absence of either light, triethylamine, air, or oxygen (Table 1 entries 2–4). This suggests that light, triethylamine and oxygen are indispensable

Table 2 Expansion of arylboronic acid substrates

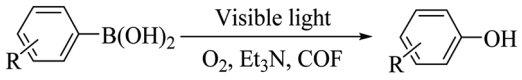


| Entry | Arylboronic acid | Product | Time (h) | Yield (%) |
|---|---|---|---|---|
| 1 | 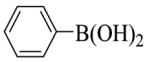 | 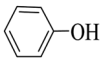 | 26 | 93 |
| 2 | 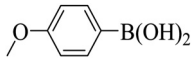 | 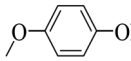 | 20 | 92 |
| 3 | 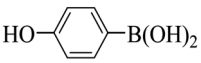 | 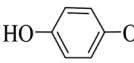 | 24 | 85 |
| 4 | 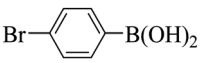 | 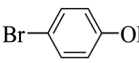 | 20 | 96 |
| 5 | 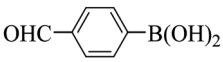 | 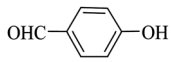 | 24 | 90 |
| 6 | 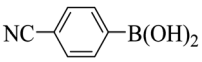 | 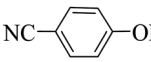 | 12 | 94 |
| 7 | 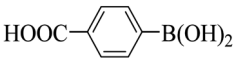 | 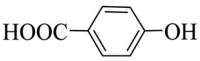 | 14 | 96 |
| 8 | 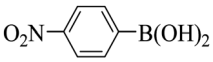 | 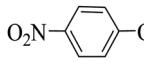 | 12 | 95 |
| 9 | 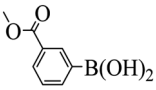 | 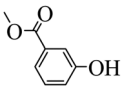 | 14 | 95 |
| 10 | 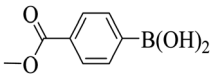 | 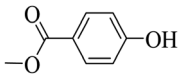 | 14 | 96 |
| 11 | 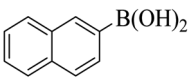 | 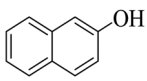 | 20 | 82 |

in the reaction. In a word, under blue light irradiation with **BTT-BTDDA-COF** as a photocatalyst, the phenylboronic acid has been successfully converted into phenol.

Subsequently, on the basis of catalytic oxidation of arylboronic acid, we further summarized the reaction range of **BTT-BTDDA-COF** photocatalytic arylboronic acid. As shown in Table 2, arylboronic acid can be well converted into the corresponding hydroxylation compounds regardless of whether the substitution groups are electron-deficient groups or electron-donating groups, and high yields can be obtained. It is noteworthy that the reaction rate of the electron-deficient group is faster than that of the electron-substituted arylboronic acid. This may be because superoxide anions can more easily access the vacant P orbitals of boron atoms in arylboronic acid containing electron-deficient substituents.[1] In addition, 2-naphthol boric acid also showed good reactivity and yielded 2-naphthol with 82% yield (Table 2, entry 11).

### 3.9 Research on catalytic mechanism

In the control experiment, we found that the photocatalytic reaction in a nitrogen atmosphere took place with only a small amount of transformation. Therefore, we hypothesize that $O_2$ plays an important role in the reaction. Previous studies have reported that covalent organic frameworks can generate superoxide radical anions using solutions in visible light.[60,70] To verify the presence of superoxide radicals in the reaction, benzoquinone was added as a free radical scavenger (Table 1, item 5). After 26 h of reaction, only 20% of arylboronic acid had been transformed. Therefore, based on previous work,[10,61,62] we proposed the hydroxylation mechanism of arylboronic acid, as shown in Fig. 5. The excited state **BTT-BTDDA-COF** * produced under visible light irradiation, through the single electron transfer (SET) process to extract an electron from triethylamine, became **BTT-BTDDA-COF**$^{\bullet-}$ and $Et_3N^{\bullet+}$. Subsequently, **BTT-BTDDA-COF**$^{\bullet-}$ is oxidized by $O_2$ to **BTT-BTDDA-COF**, which participates in the next catalytic cycle. At the same time, superoxide anion $O_2^{\bullet-}$ is added to the vacant orbital of boron in arylboronic acid to form the intermediate peroxide radical **A**. The intermediate **A** then grabs an H atom from $Et_3N^{\bullet+}$ to form peroxide **B**. After that, the intermediate **B** loses an $OH^-$ ion and rearranges to form **C**. Finally, the final phenol product **D** was obtained by hydrolysis of intermediate **C**.

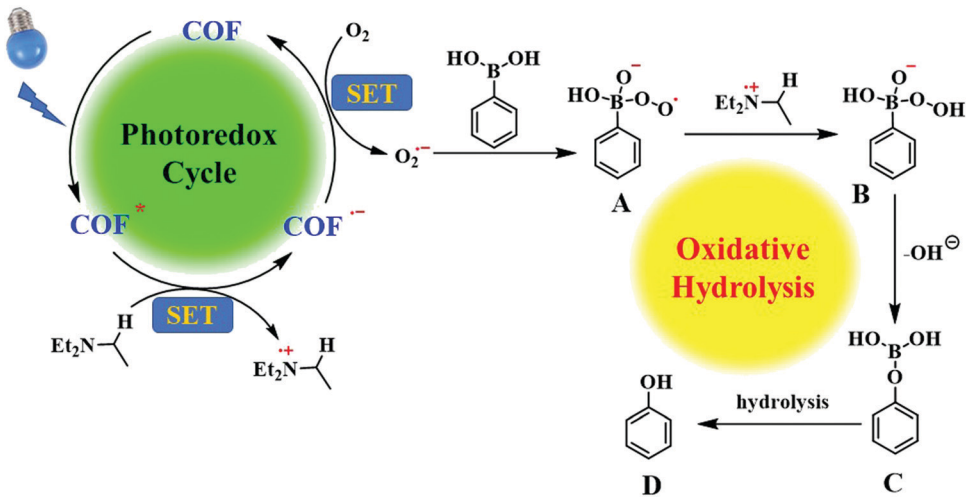


Fig. 5 Possible reaction mechanism.

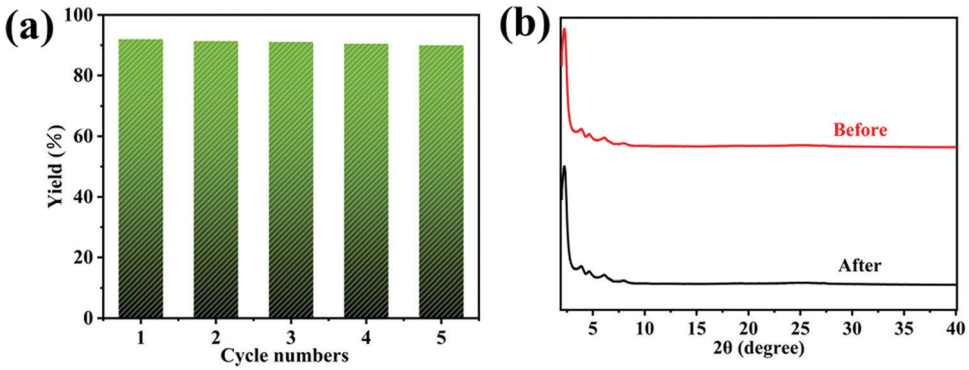


Fig. 6 (a) Repeatability of **BTT-BTDDA-COF** in photocatalytic reactions; (b) XRD pattern before and after the reaction.

### 3.10 Analysis of recyclability and catalytic performance

For catalysts, cycling stability is also one of the indicators of excellent performance. Therefore, the cycling performance of the catalyst was tested. After the reaction, the **BTT-BTDDA-COF** was centrifuged and washed with dichloromethane to ensure that no reaction substrate remained. The solid obtained was vacuum-dried at 100 °C and used for the next catalysis. To our delight, **BTT-BTDDA-COF** has a stable catalytic effect and can still maintain a good yield after 5 cycles (Fig. 6(a)), and XRD (Fig. 6(b)), FT-IR (Fig. S5, ESI†) and SEM (Fig. S6, ESI†) showed that the morphology, crystallinity and structure of the recovered **BTT-BTDDA-COF** catalyst did not change significantly. The **BTT-BTDDA-COF** catalyst has a stable spatial structure. In addition, we summarized the related organic polymers involved in the photocatalytic conversion of arylboronic acid to phenol in recent years (Table 3), and found that **BTT-BTDDA-COF** has obvious advantages.

## 4. Conclusions

In summary, we have successfully synthesized a novel D–A type covalent organic framework with high crystallinity, good stability and a wide range of visible light absorption. More importantly, **BTT-BTDDA-COF** shows high photocatalytic activity for the conversion of arylboronic acid to phenol, and can be reused many times without obvious loss of photocatalytic efficiency. This work paves the way for the design and construction of COF solid catalysts at the molecular level in the future, as well as its wider application in the field of organic transformation.

Table 3 Comparison of the performance of related organic polymers

| Entry | Catalyst | Time (h) | Yield (%) | Ref. |
|---|---|---|---|---|
| 1 | LZU-190 | 72 | 88 | 61 |
| 2 | BBO-COF | 96 | 99 | 60 |
| 3 | 3D-COF 1c | 72 | 40 | 64 |
| 4 | Tx-COF-2 | 72 | 74 | 39 |
| 5 | Cz-POF-1 | 24 | 28 | 62 |
| 6 | *g*-$C_3N_4$LMPET | 12 | 42 | 63 |
| 7 | CPOP-28 | 48 | 76 | 65 |
| 8 | BTT-BTDDA-COF | 26 | 93 | This work |

## Conflicts of interest

There are no conflicts to declare.

## References

1 B. A. Simmons, R. Ray, H. Yang and K. P. Gallagher, *Science*, 2021, **371**, 468–470.
2 Z. Song, J. Liu and H. Yang, *Appl. Energy*, 2021, **298**, 117247.
3 S. Roy, *J. Phys. Chem. C*, 2020, **124**, 28345–28358.
4 J. Li, Y. Lin, R. Chen, X. Zhu, D. Ye, Y. Yang, Y. Yu, D. Wang and Q. Liao, *J. Energy Storage*, 2021, **43**, 103228.
5 H. T. Kim, S.-Y. Lee, A. Slaoui, A. Dinia, H. J. Jeon and C. Park, *Mater. Chem. Phys.*, 2021, **265**, 124513.
6 Z. Guo, J. Wang, Y. Wang, J. Wang, J. Li, T. Mei, J. Qian and X. Wang, *Chem. Eng. J.*, 2022, **427**, 131008.
7 O. Bettucci, T. Skaltsas, M. Calamante, A. Dessì, M. Bartolini, A. Sinicropi, J. Filippi, G. Reginato, A. Mordini, P. Fornasiero and L. Zani, *ACS Appl. Energy Mater.*, 2019, **2**, 5600–5612.
8 H. Katsumata, T. Sakai, T. Suzuki and S. Kaneco, *Ind. Eng. Chem. Res.*, 2014, **53**, 8018–8025.
9 A. S. Morshedy, H. M. Abd El Salam, A. M. A. El Naggar and T. Zaki, *Energy Fuels*, 2020, **34**, 11660–11669.
10 Z. J. Wang, R. Li, K. Landfester and K. A. I. Zhang, *Polymer*, 2017, **126**, 291–295.
11 Y. Zhi, S. Ma, H. Xia, Y. Zhang, Z. Shi, Y. Mu and X. Liu, *Appl. Catal., B*, 2019, **244**, 36–44.
12 S. Wang, Q. Sun, W. Chen, Y. Tang, B. Aguila, Y. Pan, A. Zheng, Z. Yang, L. Wojtas, S. Ma and F.-S. Xiao, *Matter*, 2020, **2**, 416–427.
13 S. Yang, X. Li, Y. Qin, Y. Cheng, W. Fan, X. Lang, L. Zheng and Q. Cao, *ACS Appl. Mater. Interfaces*, 2021, **13**, 29471–29481.
14 F. Su, S. C. Mathew, L. Mohlmann, M. Antonietti, X. Wang and S. Blechert, *Angew. Chem.*, 2011, **50**, 657–660.
15 J. L. Shi, R. Chen, H. Hao, C. Wang and X. Lang, *Angew. Chem.*, 2020, **59**, 9088–9093.
16 Z. J. Wang, S. Ghasimi, K. Landfester and K. A. I. Zhang, *J. Mater. Chem. A*, 2014, **2**, 18720–18724.
17 L. Niu, X. Zhao, F. Wu, H. Lv, Z. Tang, W. Liang, X. Wang and J. Giesy, *Chem. Eng. J.*, 2021, **414**, 128619.
18 G. B. Damas, C. F. N. Marchiori and C. M. Araujo, *J. Phys. Chem. C*, 2019, **123**, 25531–25542.

19 A. M. Elewa, M. H. Elsayed, A. F. M. El-Mahdy, C.-L. Chang, L.-Y. Ting, W.-C. Lin, C.-Y. Lu and H.-H. Chou, *Appl. Catal., B*, 2021, **285**, 119802.
20 K. Feng, H. Hao, F. Huang, X. Lang and C. Wang, *Mater. Chem. Front.*, 2021, **5**, 2255–2260.
21 Q. Li, J. Wang, Y. Zhang, L. Ricardez-Sandoval, G. Bai and X. Lan, *ACS Appl. Mater. Interfaces*, 2021, **13**, 39291–39303.
22 M. Tian, Y. Wang, X. Bu, Y. Wang and X. Yang, *Catal. Sci. Technol.*, 2021, **11**, 4272–4279.
23 Z. Li, Y. Zhi, P. Shao, H. Xia, G. Li, X. Feng, X. Chen, Z. Shi and X. Liu, *Appl. Catal., B*, 2019, **245**, 334–342.
24 G. B. Wang, S. Li, C. X. Yan, Q. Q. Lin, F. C. Zhu, Y. Geng and Y. B. Dong, *Chem. Commun.*, 2020, **56**, 12612–12615.
25 W. Huang, B. C. Ma, D. Wang, Z. J. Wang, R. Li, L. Wang, K. Landfester and K. A. I. Zhang, *J. Mater. Chem. A*, 2017, **5**, 3792–3797.
26 Y. Zhi, Z. Li, X. Feng, H. Xia, Y. Zhang, Z. Shi, Y. Mu and X. Liu, *J. Mater. Chem. A*, 2017, **5**, 22933–22938.
27 Z. Liu, Q. Su, P. Ju, X. Li, G. Li, Q. Wu and B. Yang, *Chem. Commun.*, 2020, **56**, 766–769.
28 S. Liu, W. Pan, S. Wu, X. Bu, S. Xin, J. Yu, H. Xu and X. Yang, *Green Chem.*, 2019, **21**, 2905–2910.
29 X. Kang, X. Wu, X. Han, C. Yuan, Y. Liu and Y. Cui, *Chem. Sci.*, 2019, **11**, 1494–1502.
30 H. Zhang, Q. Huang, W. J. Zhang, C. Y. Pan, J. Wang, C. X. Ai, J. T. Tang and G. P. Yu, *ChemPhotoChem*, 2019, **3**, 645–651.
31 Z. J. Wang, K. Garth, S. Ghasimi, K. Landfester and K. A. Zhang, *ChemSusChem*, 2015, **8**, 3459–3464.
32 W.-K. An, S.-J. Zheng, Y.-N. Du, S.-Y. Ding, Z.-J. Li, S. Jiang, Y. Qin, X. Liu, P.-F. Wei, Z.-Q. Cao, M. Song and Z. Pan, *Catal. Sci. Technol.*, 2020, **10**, 5171–5180.
33 Z. Li, S. Han, C. Li, P. Shao, H. Xia, H. Li, X. Chen, X. Feng and X. Liu, *J. Mater. Chem. A*, 2020, **8**, 8706–8715.
34 S. Han, Z. Li, S. Ma, Y. Zhi, H. Xia, X. Chen and X. Liu, *J. Mater. Chem. A*, 2021, **9**, 3333–3340.
35 Z. Almansaf, J. Hu, F. Zanca, H. R. Shahsavari, B. Kampmeyer, M. Tsuji, K. Maity, V. Lomonte, Y. Ha, P. Mastrorilli, S. Todisco, M. Benamara, R. Oktavian, A. Mirjafari, P. Z. Moghadam, A. R. Khosropour and H. Beyzavi, *ACS Appl. Mater. Interfaces*, 2021, **13**, 6349–6358.
36 J. Yuan, Q. Xia, W. Zhu, C. Wu, B. Wang, B. Liu, X. Yang, Y. Xu and H. Xu, *ChemPhotoChem*, 2020, **4**, 445–450.
37 Z. Dong, L. Zhang, J. Gong and Q. Zhao, *Chem. Eng. J.*, 2021, **403**, 126383.
38 K. Lei, D. Wang, L. Ye, M. Kou, Y. Deng, Z. Ma, L. Wang and Y. Kong, *ChemSusChem*, 2020, **13**, 1725–1729.
39 Y. Nailwal, A. D. D. Wonanke, M. A. Addicoat and S. K. Pal, *Macromolecules*, 2021, **54**, 6595–6604.
40 X. Lan, X. Liu, Y. Zhang, Q. Li, J. Wang, Q. Zhang and G. Bai, *ACS Catal.*, 2021, **11**, 7429–7441.
41 H. Liu, C. Li, H. Li, Y. Ren, J. Chen, J. Tang and Q. Yang, *ACS Appl. Mater. Interfaces*, 2020, **12**, 20354–20365.
42 E. Jin, Z. Lan, Q. Jiang, K. Geng, G. Li, X. Wang and D. Jiang, *Chem*, 2019, **5**, 1632–1647.
43 C. Lin, X. Liu, B. Yu, C. Han, L. Gong, C. Wang, Y. Gao, Y. Bian and J. Jiang, *ACS Appl. Mater. Interfaces*, 2021, **13**, 27041–27048.
44 L. Guo, Y. Niu, H. Xu, Q. Li, S. Razzaque, Q. Huang, S. Jin and B. Tan, *J. Mater. Chem. A*, 2018, **6**, 19775–19781.
45 S. Li, L. Li, Y. Li, L. Dai, C. Liu, Y. Liu, J. Li, J. Lv, P. Li and B. Wang, *ACS Catal.*, 2020, **10**, 8717–8726.
46 P. Pachfule, A. Acharjya, J. Roeser, R. P. Sivasankaran, M. Y. Ye, A. Bruckner, J. Schmidt and A. Thomas, *Chem. Sci.*, 2019, **10**, 8316–8322.
47 W. Li, X. Huang, T. Zeng, Y. A. Liu, W. Hu, H. Yang, Y. B. Zhang and K. Wen, *Angew. Chem.*, 2021, **60**, 1869–1874.
48 W. Hao, D. Chen, Y. Li, Z. Yang, G. Xing, J. Li and L. Chen, *Chem. Mater.*, 2019, **31**, 8100–8105.
49 J.-l. Wang, G. Ouyang, D. Wang, J. Li, J. Yao, W.-S. Li and H. Li, *Macromolecules*, 2021, **54**, 2661–2666.
50 Y. Zhang, G. Wu, H. Liu, R. Tian, Y. Li, D. Wang, R. Chen, J. Zhao, S. Liu, Z. Li and Y. Zhao, *Mater. Chem. Front.*, 2021, **5**, 6575–6581.
51 R. Wang, Q. Cai, Y. Zhu, Z. Mi, W. Weng, Y. Liu, J. Wan, J. Hu, C. Wang, D. Yang and J. Guo, *Chem. Mater.*, 2021, **33**, 3566–3574.
52 Z. Lu, X. Fu, H. Yang, Y. Zhao, L. Xiao and L. Hou, *Polym. Chem.*, 2021, **12**, 183–188.
53 Q. Liao, W. Xu, X. Huang, C. Ke, Q. Zhang, K. Xi and J. Xie, *Sci. China: Chem.*, 2020, **63**, 707–714.
54 J. Yu, X. Sun, X. Xu, C. Zhang and X. He, *Appl. Catal., B*, 2019, **257**, 117935.
55 G. B. Wang, F. C. Zhu, Q. Q. Lin, J. L. Kan, K. H. Xie, S. Li, Y. Geng and Y. B. Dong, *Chem. Commun.*, 2021, **57**, 4464–4467.
56 W. Chen, Z. Yang, Z. Xie, Y. Li, X. Yu, F. Lu and L. Chen, *J. Mater. Chem. A*, 2019, **7**, 998–1004.
57 H. Li, P. Shao, S. Chen, G. Li, X. Feng, X. Chen, H. J. Zhang, J. Lin and Y. B. Jiang, *J. Am. Chem. Soc.*, 2020, **142**, 3712–3717.
58 S. Bi, P. Thiruvengadam, S. Wei, W. Zhang, F. Zhang, L. Gao, J. Xu, D. Wu, J. S. Chen and F. Zhang, *J. Am. Chem. Soc.*, 2020, **142**, 11893–11900.
59 B. Luo, Y. Chen, Y. Zhang and J. Huo, *J. Catal.*, 2021, **402**, 52–60.
60 X. Yan, H. Liu, Y. Li, W. Chen, T. Zhang, Z. Zhao, G. Xing and L. Chen, *Macromolecules*, 2019, **52**, 7977–7983.
61 P. F. Wei, M. Z. Qi, Z. P. Wang, S. Y. Ding, W. Yu, Q. Liu, L. K. Wang, H. Z. Wang, W. K. An and W. Wang, *J. Am. Chem. Soc.*, 2018, **140**, 4623–4631.
62 J. Luo, X. Zhang and J. Zhang, *ACS Catal.*, 2015, **5**, 2250–2254.
63 T. Xu, W. Lu, X.-F. Wu and W. Chen, *J. Catal.*, 2019, **378**, 63–67.
64 A. Jiménez-Almarza, A. López-Magano, L. Marzo, S. Cabrera, R. Mas-Ballesté and J. Alemán, *ChemCatChem*, 2019, **11**, 4916–4922.
65 H.-P. Liang, Q. Chen and B.-H. Han, *ACS Catal.*, 2018, **8**, 5313–5322.
66 Z.-Y. Xu, Y. Luo, D.-W. Zhang, H. Wang, X.-W. Sun and Z.-T. Li, *Green Chem.*, 2020, **22**, 136–143.
67 W. Huang, Q. He, Y. Hu and Y. Li, *Angew. Chem.*, 2019, **58**, 8676–8680.
68 Y. S. Kochergin, K. Villa, F. Novotný, J. Plutnar, M. J. Bojdys and M. Pumera, *Adv. Funct. Mater.*, 2020, **30**, 2002701.
69 Z. Zhao, Y. Zheng, C. Wang, S. Zhang, J. Song, Y. Li, S. Ma, P. Cheng, Z. Zhang and Y. Chen, *ACS Catal.*, 2021, **11**, 2098–2107.
70 J. A. Johnson, J. Luo, X. Zhang, Y.-S. Chen, M. D. Morton, E. Echeverría, F. E. Torres and J. Zhang, *ACS Catal.*, 2015, **5**, 5283–5291.